Smart Energy System Research

SCIEPublish

Article

Empirical Evaluation of Service-Enriched EV and Building Flexibility Contracts in Distribution Feeders

Divine Okeke *, Elena Gryazina and Federico M. Ibanez

Center for Energy Science and Technology, Skolkovo Institute of Science and Technology, Bolshoy Boulevard 30, bld. 1, Moscow 121205, Russia; e.gryazina@skoltech.ru (E.G.); fm.ibanez@skoltech.ru (F.M.I.)

* Corresponding author. E-mail: divine.okeke@skoltech.ru (D.O.)

Received: 1 August 2026; Revised: 21 August 2026; Accepted: 14 September 2026; Available online: 23 September 2026

ABSTRACT: Electric-vehicle (EV) charging and flexible building loads can increase or relieve distribution-level loading and voltage stress, depending on timing, placement, and flexibility. This paper empirically evaluates a shared service-enriched flexibility-contract representation for coordinating EV departure-energy service and building comfort service. Individual EV and building records encode service limits, deadlines or comfort bounds, and feeder locations. The evaluation compares uncontrolled, service-constrained, feeder-aware, and heuristic uncertainty-aware control, with inputs from empirical residuals or split-conformal scalar service-score quantiles. In the simplified study, 256 scenarios under four modes produce 1024 evaluations. Realized nominal EV energy shortfall and building comfort violations are zero in the tested scenarios, while a separate earlier-departure stress audit shows heuristic uncertainty-aware tightening reducing EV stress-risk cases from 106 to 64. Open Distribution System Simulator (OpenDSS) audits on IEEE 123 and IEEE 34 each include 2048 scenarios and 8192 evaluations; stress-risk cases fall from 1005 to 536, with mean peak tradeoffs of 17.66 kW and 18.26 kW. A reduced-information experiment compares raw-state, individual-contract, and noisy/coarsened information-view proxies for exposure and payload rather than formal privacy. The results provide bounded empirical evidence that service-enriched EV/building contracts can expose service-grid and information-view tradeoffs in the tested simplified and OpenDSS feeder studies and audits.

Keywords: Active distribution networks; Electric-vehicle charging; Building flexibility; Service contracts; Distribution feeders; Heuristic uncertainty-aware control; Open Distribution System Simulator; Information-view proxies

1. Introduction

Electric-vehicle (EV) adoption changes distribution-feeder operating conditions in ways that depend on both time and place. Temporally concentrated charging can increase residential or workplace peaks, while feeder location, phase connection, and charging strategy affect line and transformer loading, voltage profiles, losses, and imbalance in the studied networks [1–6]. Flexible building loads can help reshape demand, but their grid value also depends on weather, occupancy, feeder placement, and the timing of flexibility. Distribution-level coordination, therefore, needs service and feeder audit metrics rather than only aggregate energy-balance metrics.

EV flexibility is service-bounded because a vehicle is useful to the grid only while it is connected and only to the extent that charging still satisfies the user's requested energy by departure. Arrival time, departure or dwell time, requested energy, charger rating, and site behavior vary across sessions, and prior EV charging work already models such service and availability constraints in centralized, decentralized, data-driven, and feeder-aware settings [7–14]. As a result, EV demand cannot be treated as unrestricted load shifting; the service semantics include availability, power, energy, deadline, and location.

Building and thermostatically controlled load (TCL) flexibility introduces different service semantics. Thermal inertia can make heating, ventilation, and air conditioning (HVAC) and other TCL demand useful for load following, energy arbitrage, and aggregate flexibility, but the usable flexibility is constrained by comfort bands, thermal dynamics, weather forecasts, and model sensitivity [15–19]. Building comfort is therefore not the same service as EV departure energy, even though both can be represented as flexibility with service-relevant bounds. Building comfort is treated as a second service obligation in the evaluation.

The information needed to coordinate these resources can be operationally sensitive or burdensome to exchange. EV session histories, requested energy, customer timing patterns, building thermal states, and comfort information may all be useful for control, yet reduced-information coordination, formal privacy mechanisms, flexibility envelopes, dynamic operating envelopes, and information-value studies are already established in related literature [14,20–25]. This paper therefore studies a shared service-enriched contract representation and raw-state, individual-contract, and noisy/coarsened information-view proxies. These proxies measure declared information exposure and payload.

Prior work covers EV service-aware charging, building/TCL comfort flexibility, joint EV/TCL coordination, flexibility envelopes, uncertainty-aware control, reduced-information or privacy-aware coordination, and conformal calibration [13,17,24–27]. The existing literature establishes the individual ingredients, while this study evaluates EV/building service semantics, uncertainty inputs, information-view proxies, and feeder-audit outcomes together in one empirical workflow. The gap addressed here is the combined empirical evaluation of EV departure-energy and building comfort service semantics within one shared representation, with uncertainty inputs, information-view proxies, and feeder-level audits evaluated together. The primary research question is: what service-grid and information-view tradeoffs are observed for a shared EV/building service-enriched contract representation under heuristic uncertainty inputs populated from empirical residuals or split-conformal scalar service-score quantiles in simplified and OpenDSS feeder audits?

This paper makes two contributions:

1. We implement a shared service-enriched EV/building representation that encodes EV departure-energy/deadline service and building comfort/thermal service, with feeder bus/phase labels and summaries, within an individual-agent feeder simulation and audit workflow.
2. We empirically evaluate how the shared representation exposes service-grid, uncertainty-input, feeder-audit, and information-view tradeoffs across a 256-scenario simplified matrix and two 2048-scenario OpenDSS feeder matrices, supplemented by focused information-view, conformal-input, and linearized optimization-aware analyses.

Section 6 states the implementation and inference boundaries.

2. Related Work and Positioning

2.1. EV and Building Service-Aware Flexibility Coordination

Coordinated EV charging already models many of the service quantities used in this study: arrival and departure times, requested energy, charging-rate limits, owner or charging-session constraints, feeder congestion or voltage impacts, and session uncertainty [6–8,11,12]. Yan, Ma, and Chen derive a stronger formal aggregate EV power flexibility region for charging stations, including alternating-current (AC)-network coordination, and show a feasible disaggregation from aggregate-region schedules to EV charging strategies [13]. Winschermann et al. separately show that the value of detailed EV information can be measured for office-building charging strategies [14]. This paper, therefore, does not claim EV service-aware charging or reduced-information EV coordination as standalone contributions; EV departure-energy and deadline fields are one service semantic in the shared EV/building representation evaluated here.

Building and thermostatically controlled load (TCL) flexibility is also mature. Thermal inertia, comfort bands, weather forecasts, aggregate flexibility, virtual-battery representations, and quality-of-service constraints have been studied for load following, arbitrage, regulation, and building climate control [15–19]. Hao et al. provide a rigorous aggregate TCL flexibility model through generalized and stochastic battery representations [17]. Joint EV and TCL/HVAC coordination is likewise established: Liu et al. coordinate aggregated EVs and TCLs within hierarchical energy systems subject to EV and comfort constraints [26]. The present study consequently does not claim building comfort, flexibility, or joint EV/TCL coordination as standalone contributions; it uses building comfort and thermal-service fields as the building-side counterpart to EV departure-energy service in one empirical feeder workflow.

2.2. Flexibility Envelopes and Distribution-System Interfaces

The contract records in this paper sit within a long line of flexibility-envelope and operating-envelope interfaces rather than outside it. Nosair and Bouffard establish flexibility envelopes for power-system operational planning [24]. Fan and Kockar formulate local flexibility offers for unbalanced distribution-network operation [28]. Yan, Ma, and Chen provide aggregate EV flexibility regions with stronger formal feasibility and disaggregation properties than the EV representation used here [13]. Liu and Braslavsky compute robust dynamic operating envelopes for distributed energy resource (DER) integration in unbalanced distribution networks, giving a stronger network-feasibility and uncertainty formulation than this manuscript's feeder-aware heuristic and ex-post audit [25]. Tostado-Veliz et al. recently constructed preference-aware flexibility envelopes for coordinated energy-community operation, further establishing service- or preference-aware envelopes and limited-information distribution system operator (DSO) interfaces [29].

These studies already cover flexibility envelopes, aggregate flexibility regions, operating envelopes, nodal or phase-aware flexibility, preference-aware envelopes, reduced-information coordination, and stronger network-feasibility formulations. The distinction is the service-specific EV/building implementation and empirical feeder workflow: EV departure-energy/deadline and building comfort/thermal service are evaluated together with feeder-audit and information-view outcomes. This positioning retains the envelope literature as context rather than claiming a new envelope theory or DSO-interface method.

2.3. Uncertainty, Conformal Calibration, and Feeder Evaluation

Uncertainty-aware coordination has a deeper formal literature than the heuristic tightening used in this manuscript. Building model predictive control (MPC) and weather-aware control, robust and stochastic power-system optimization, chance-constrained formulations, distributionally robust methods, robust/explicit model predictive control (eMPC) EV charging, and operating-envelope uncertainty methods provide mathematically stronger treatments of forecast, availability, load, generation, and network uncertainty [12,16,25,30,31]. In contrast, the uncertainty-aware controller studied here applies heuristic service-margin and reserve rules whose inputs are configured from empirical residuals or scalar score quantiles; it does not provide a robust, stochastic, chance-constrained, or network-security guarantee.

Conformal prediction is likewise established before this study. Vovk et al. provide the foundational framework, Angelopoulos and Bates give a modern tutorial treatment, and Renkema, Brinkel, and AlSkaif apply conformal prediction to stochastic decision-making for photovoltaic (PV) power in electricity markets [27,32,33]. This manuscript does not propose a conformal method. It maps split-conformal scalar service-score quantiles into existing heuristic uncertainty/configuration inputs. The resulting evidence should not be read as a joint EV/building conformal guarantee, a conditional coverage result, or a feeder-security guarantee. Similarly, OpenDSS and IEEE test feeders are used here as ex-post feeder audit and evaluation tools [34–36]; the unbalanced feeder evaluation serves as supporting evidence, not a separate contribution.

2.4. Data Minimization, Privacy-Aware Coordination, and This Study's Empirical Scope

Reduced-information coordination and formal privacy-aware energy methods are also established. Yan, Ma, and Chen reduce detailed EV data exchange through aggregate flexibility regions [13]. Smart-meter privacy work identifies the sensitivity of load data [20]; secure and privacy-preserving aggregation and differential-privacy mechanisms have been developed for metering and demand-side management [21–23]. Winschermann et al. quantify the value of EV charging information [14], while Tostado-Veliz et al. present a recent preference-aware envelope approach that limits detailed DSO access [29]. These works are stronger than this manuscript on formal privacy or reduced-information theory, where they provide explicit mechanisms, guarantees, or feasibility results.

This study evaluates information-view and exposure/payload proxies; the grouped/noisy payload accounts for output rather than a dispatch input. Its scope is the empirical EV/building feeder workflow, not a formal privacy or reduced-information control mechanism. Prior work, therefore, establishes each of the main ingredients individually, while this study evaluates EV/building service semantics, uncertainty inputs, information-view proxies, and feeder-audit outcomes together in one empirical workflow.

3. Material and Methods

3.1. Service-Contract Simulation Architecture

Figure 1 summarizes the conceptual architecture, but the executable boundary is more specific. The current implementation is a monolithic individual-agent simulation in which service-contract records and bus/phase summaries are generated as coordination, diagnostic, and evaluation representations, while controller functions retain access to the full seeded SmokeScenario, individual EV agents, individual building/TCL agents, base-load profiles, uncertainty settings, and feeder-sensitivity interface. Thus, the executable scheduler is not a serialized-contract-only or aggregate-only controller. Individual EV and building contracts are generated with bus and phase labels; bus/phase summaries are formed for reporting and selected optimization-aware cost terms; dispatch profiles and OpenDSS feeder evaluation remain based on individual agent-load records.

The implementation-information flow is:

raw scenario/agent state
→ individual service-contract records
→ {bus/phase summaries; information-view and payload accounting}.

The same simulation then schedules individual agents and passes individual load profiles to the feeder evaluator. This distinction is important for interpreting the reduced-information studies: they compare declared information views and serialized payload/exposure proxies, not an operational privacy-preserving or aggregate-contract dispatch architecture.

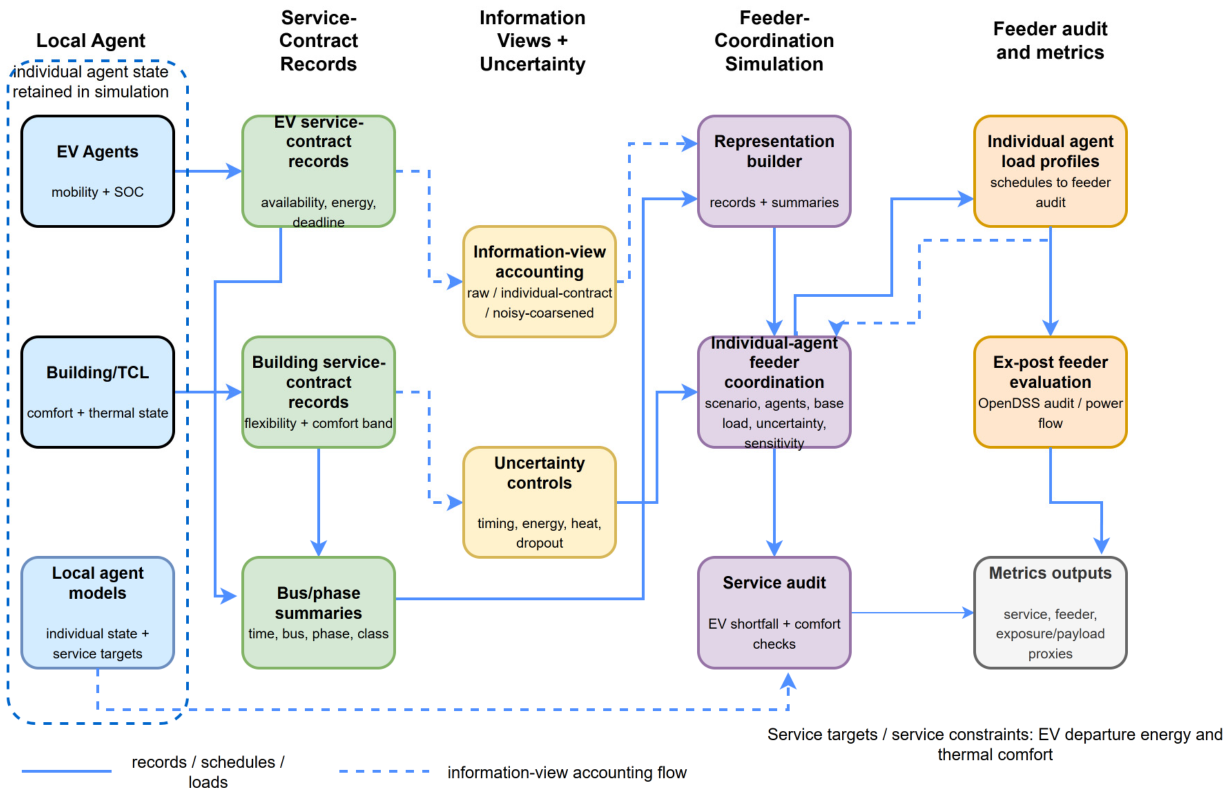

Figure 1. Service-contract simulation and feeder-evaluation architecture for electric-vehicle (EV) and thermostatically controlled-load (TCL) studies. The implementation generates service-contract records and bus/phase summaries, schedules individual agents, audits individual load records ex post, and separately records raw-state, individual-contract, and noisy/coarsened information views; SOC: state of charge; OpenDSS: Open Distribution System Simulator.

3.2. Local Service Models

The coordination horizon is indexed by $t \in \mathcal{T} = \{1, \ldots, T\}$ with timestep length Δt in hours and Δt_m in minutes. EV agents are indexed by $i \in \mathcal{E}$ and building/TCL agents by $j \in \mathcal{B}$. Each flexible agent is assigned to a feeder service point (b, ϕ), where $b \in \mathcal{N}$ is a bus and $\phi \in \Phi = \{a, b, c\}$ is a phase. The base feeder load is denoted P_t^0.

For EV i, let $p_{i,t}^{EV}$ be charging power, a_i and d_i the arrival and departure timesteps, $\bar{p}_i$ the charger rating, E_i^{req} the required delivered energy derived from the target state of charge, initial state of charge, and battery capacity, and m_i^E an optional controller-side planning reserve. The availability indicator is $\alpha_{i,t} = 1$ for $a_i \le t < d_i$ and zero otherwise. The generated EV service-contract record contains the agent identifier, bus, phase, start and end timestep, lower and upper feasible-power profiles, a priority label, required departure energy, departure timestep, and charger rating. In the current contract generator, the stored per-timestep uncertainty-margin field is a zero placeholder; implemented reserve tightening is instead read from the scenario/controller uncertainty configuration. A service-feasible EV schedule satisfies.

$$0 \le p_{i,t}^{EV} \le \alpha_{i,t}\bar{p}_i, \quad \forall i, t, \tag{1}$$

$$\sum_{t \in \mathcal{T}} p_{i,t}^{EV}\, \Delta t \ge E_i^{req} + m_i^E, \tag{2}$$

when a tightened target is used and feasible. The nominal audit shortfall is computed over the actual arrival-to-departure interval as $s_i^E = \max\{0, E_i^{req} - \sum_{t=a_i}^{d_i-1} p_{i,t}^{EV}\, \Delta t\}$. The simulator retains the individual EV object, including SOC-derived requested energy and timing fields; the manuscript therefore treats contract records as an implemented representation, not as proof that raw EV state is unavailable to the executable controller.

For building/TCL agent j, let $p^{B}_{j,t}$ be the total building power, $\bar{p}^{base}_{j}$ the non-HVAC base power, $u_{j,t} \in \{0,1\}$ the local HVAC action, $\bar{p}^{hvac}_{j}$ the HVAC rating, $T_{j,t}$ the indoor temperature, T^{out}_{t} the outdoor temperature, and $[T^{min}_{j}, T^{max}_{j}]$ the comfort band. The implemented local reduced-order model is

$$\begin{gathered} p^{B}_{j,t} = \bar{p}^{base}_{j} + \bar{p}^{hvac}_{j} u_{j,t}, \\ T_{j,t+1} = T_{j,t} + \Delta t\big[g_j \max(0, T^{out}_{t} - T_{j,t}) - c_j u_{j,t}\big], \end{gathered} \tag{3}$$

with envelope gain g_j and cooling coefficient c_j retained locally. Feasible building service requires

$$T^{min}_{j} - s^{-}_{j,t} \le T_{j,t} \le T^{max}_{j} + s^{+}_{j,t}, \quad s^{-}_{j,t}, s^{+}_{j,t} \ge 0, \tag{4}$$

and the reported comfort violation is the sum of degree-minutes outside the comfort band. The generated building contract contains the agent identifier, bus, phase, start and end timestep, base-to-base-plus-HVAC power envelope, comfort minimum and maximum, thermal slack, restore-by timestep, priority label, and a zero uncertainty-margin placeholder. The executable building controller still calls individual building methods that use local thermal coefficients and the indoor temperature state. The agent model does not include occupancy state.

3.3. Service-Contract Coordination Formulation

Each EV or building contract k exposes lower and upper feasible power limits, a priority class, and a service point (b_k, ϕ_k). The contract data structure also includes an uncertainty-margin field $\mu_{k,t}$, but generated contract margins are zero in this implementation. Bus/phase summaries are computed as

$$\underline{P}_{b,\phi,t} = \sum_{k: b_k = b, \phi_k = \phi} \underline{p}_{k,t}, \quad \overline{P}_{b,\phi,t} = \sum_{k: b_k = b, \phi_k = \phi} \overline{p}_{k,t}, \tag{5}$$

and the realized flexible-load summaries are reported as

$$P^{flex}_{b,\phi,t} = \sum_{i: b_i = b, \phi_i = \phi} p^{EV}_{i,t} + \sum_{j: b_j = b, \phi_j = \phi} p^{B}_{j,t}. \tag{6}$$

The total load and phase load proxies are

$$P_t = P^{0}_{t} + \sum_{b,\phi} P^{flex}_{b,\phi,t}, \quad P_{\phi,t} = P^{0}_{t}/|\Phi| + \sum_{b} P^{flex}_{b,\phi,t}. \tag{7}$$

Equations (5)–(7) define summary and accounting quantities. They are not hard aggregate dispatch bounds for the feeder-aware or uncertainty-aware scheduler. In the optimization-aware EV allocation, the bus/phase contract count enters a location-density term in the EV cost, but individual EV/time variables and individual building profiles are still retained.

Uncertainty-aware tightening uses arrival, departure, energy, temperature, and dropout inputs from uncertainty or controller_uncertainty configuration keys. In the implemented EV controller, the effective deadline uses rounded timesteps,

$$\tilde{d}_i = \max\left(a_i + 1, d_i - \mathrm{round}\left(\frac{\max(0, \delta^{d}_{i})}{\Delta t_m}\right)\right), \tag{8}$$

The controller converts the nonnegative departure-timing margin to a whole number of timesteps using the round operation in Equation (8).

The corresponding planning energy is

$$\tilde{E}_i^{req} = E_i^{req}(1+\rho_i), \quad \rho_i = \min\left(0.25, \frac{\delta_i^a + \delta_i^d}{240} + \epsilon_i^E + 0.25q\right), \tag{9}$$

where δ_i^a and δ_i^d are nonnegative arrival and departure timing margins in minutes, ϵ_i^E is the requested-energy error fraction, q is the communication-dropout sensitivity input, and $\tilde{\alpha}_{i,t} = 1$ for $a_i \le t < \tilde{d}_i$. The constants 240, 0.25, and the dropout coefficient 0.25 are fixed controller-design heuristics. In the feeder-aware uncertainty path, the controller tries to deliver $E_i^{req}(1+\rho_i)$ over the tightened window and then fills the original window if the tightened schedule leaves remaining energy. In the optimization-aware EV path, the target is capped by the charging capacity available in the tightened feasible window; if that capped target is below the original request, the path falls back to the original service window and caps at the original feasible energy.

For building/TCL service, the uncertainty-aware controller solves the local dynamic program under a stressed outdoor-temperature sequence

$$\tilde{T}_t^{out} = T_t^{out} + 0.5h + 1.5q, \quad h = \max(0, \delta^T) + \max(0, \sigma^T) + \max(0, \eta^T), \tag{10}$$

where δ^T is an outdoor-temperature shift, σ^T an outdoor-temperature residual scale, and η^T a thermal-model error margin. The coefficients 0.5 and 1.5 are fixed heuristics. The implemented controller also uses a risk-adjusted building stress signal,

$$\tilde{\ell}_t = \max(0, \ell_t - \min(0.45, 0.75q + 0.04h)), \tag{11}$$

and falls back to the service-constrained building profile when the building is dropped or when $q \ge 0.15$. A restore-by field is stored in the generated building contract,

$$\sum_{\tau=t}^{r_j} \left(p_{j,\tau}^B - \bar{p}_j^{base}\right)\Delta t \ge H_{j,t}^{req}, \quad t \le r_j, \tag{12}$$

where $H_{j,t}^{req}$ denotes the local cooling-energy requirement implied by the comfort dynamic program. Building feasibility is enforced by the local dynamic program and fallback logic rather than by a central aggregate restore constraint. Table 1 summarizes the parameter provenance for these uncertainty and controller settings.

Table 1. Uncertainty and controller parameters used in the executable Methods.

Quantity	Classification	Implementation Source and Role
Arrival timing margin δ^a	empirical input, split-conformal input, or scenario sensitivity assumption	uncertainty.ev_arrival_perturb_minutes or controller_uncertainty.ev_arrival_perturb_minutes; contributes to EV reserve factor but does not shift the actual arrival step in the controller.
Departure timing margin δ^d	empirical input, split-conformal input, or scenario sensitivity assumption	ev_departure_perturb_minutes; converted to timesteps by Equation (8) using round; also drives the EV earlier-departure stress audit.
Requested-energy error ϵ^E	empirical input, split-conformal input, or scenario sensitivity assumption	ev_requested_energy_error_fraction; enters Equation (9) with fixed unit coefficient.
Outdoor-temperature shift δ^T and residual scale σ^T	empirical input or scenario sensitivity assumption	outdoor_temperature_shift_c and outdoor_temperature_noise_std_c; part of heat-risk input h. In conformal service-margin configs these are set to zero, and the thermal scalar score populates η^T.
Thermal-model error η^T	empirical proxy or split-conformal scalar input	thermal_model_error_c; derived from NREL/NIST-style thermal calibration artifacts or the conformal thermal service score.

Communication dropout q	configuration constant or scenario sensitivity assumption	communication_dropout_rate; not telemetry calibrated and not conformally calibrated. It enters EV reserve, thermal temperature stress, building fallback, and risk-stress weighting.
EV reserve coefficients $240,\ 0.25,\ 0.25q$	fixed heuristic	Literal constants in _ev_reserve_factor; not learned, fitted, or conformally calibrated.
Thermal coefficients $0.5,\ 1.5$	fixed heuristic	Literal constants in the risk-temperature calculation for building/TCL scheduling.
Dropout fallback threshold 0.15	fixed heuristic	If dropout risk is at least 0.15, building/TCL scheduling uses the service-constrained local profile.
Risk-weight expression $\min(0.45, 0.75q + 0.04h)$	fixed heuristic	Reduces the stress signal used by the building dynamic program; not a calibrated reserve law.
Optimization objective weights	configuration constants	controller.objective_weights.* (where * denotes any configured objective-weight key) and controller.reserve_price_per_kwh; used only in the optimization-aware EV allocation study.

The optimization-aware mode uses a linearized EV allocation problem after local building/TCL profiles have been selected. Let z upper-bound the aggregate feeder peak and z_{ϕ} upper-bound phase-specific loading. Let γ_b be the feeder-location sensitivity returned by the feeder interface, $\ell_t = P_t^0/\max_{\tau} P_{\tau}^0$ the normalized loading signal, λ_t^X the transformer loading proxy, $\lambda_{\phi,t}^{\phi}$ the phase-pressure proxy, $n_{b,\phi}$ the local contract concentration, and $c_{i,t}$ the per-kW EV placement cost:

$$
\begin{aligned}
c_{i,t} &= w_L \ell_t + w_X \lambda_t^X + w_V \gamma_{b_i} \ell_t \\
&+ w_{\Phi}\left(\lambda_{\phi_i,t}^{\phi} + 0.1 n_{b_i,\phi_i}\right) + w_C \max(0, \ell_t - 0.65) + w_S \frac{t}{T} + w_R + \pi^R,
\end{aligned}
\tag{13}
$$

where $w_L, w_X, w_V, w_{\Phi}, w_C, w_S, w_R$ are loading, transformer, voltage, phase-imbalance, curtailment, service-slack, and reserve weights, and π^R is an optional reserve price. The solved linear program is

$$
\begin{aligned}
\min_{p^{EV}, z, z_{\phi}} \quad & \sum_{i,t} c_{i,t}\, p_{i,t}^{EV} + w_P z + w_{\Phi} \sum_{\phi} z_{\phi} \\
\text{s.t.} \quad & 0 \le p_{i,t}^{EV} \le \tilde{\alpha}_{i,t} \bar{p}_i, \quad \forall i, t, \\
& \sum_{t} p_{i,t}^{EV}\, \Delta t \ge \tilde{E}_i^{req}, \quad \forall i, \\
& P_t^{fix} + \sum_{i} p_{i,t}^{EV} \le z, \quad \forall t, \\
& P_{\phi,t}^{fix} + \sum_{i:\phi_i = \phi} p_{i,t}^{EV} \le z_{\phi}, \quad \forall \phi, t,
\end{aligned}
\tag{14}
$$

where P_t^{fix} and $P_{\phi,t}^{fix}$ include base load and local building/TCL dispatch. SciPy linear programming is used when available; otherwise, a deterministic greedy allocator fills EV energy in low-cost feasible timesteps. The formulation is optimization-aware because the allocation objective and constraints are explicit, but it is not AC optimal power flow (OPF) and does not impose hard voltage or thermal feeder-security constraints. Voltage, line-loading, transformer-loading, and phase-imbalance outcomes are evaluated ex post through OpenDSS when a feeder model is available.

The historical simplified uncertainty matrix compares four controller modes. Uncontrolled charging is immediate, and buildings follow thermostat-only behavior. Service-constrained dispatch spreads EV charging and modulates buildings while preserving local service, without feeder coordination. Feeder-aware dispatch uses the stress signal and bus sensitivity in a sequential low-stress placement heuristic. Uncertainty-aware dispatch applies Equations (8)–(11) before the feeder-aware heuristic. Optimization-aware dispatch is enabled only in separate focused analyses; it uses Equation (14) for EV allocation while keeping building/TCL dispatch in the local comfort-constrained dynamic program.

3.4. Algorithms

Algorithm 1 summarizes the individual-agent simulation and feeder-evaluation flow. Algorithm 2 summarizes the uncertainty-aware tightening flow.

Algorithm 1. Individual-agent service-contract simulation and feeder evaluation

Step	Operation
1:	Generate seeded EV, building/TCL, base-load, placement, uncertainty, and feeder metadata.
2:	Generate individual EV and building service-contract records and bus/phase summaries for representation, diagnostics, and selected objective terms.
3:	Build controller inputs from the retained individual-agent scenario, base load, uncertainty configuration, and feeder-sensitivity view.
4:	Dispatch EV and building/TCL flexibility at individual-agent granularity according to the selected controller mode.
5:	Apply heuristic uncertainty-aware reserve tightening or the separate optimization-aware EV allocation when enabled.
6:	Convert dispatch into individual AgentLoad records with agent identifier (ID), bus, phase, and profile.
7:	Evaluate dispatch through a simplified radial feeder or OpenDSS feeder model ex post.
8:	Report grid, realized service, reserve, curtailment, stress-audit, exposure-proxy, payload-proxy, and placement metrics.

Algorithm 2. Uncertainty-aware service-contract tightening

Step	Operation
1:	Convert nonnegative departure timing uncertainty into integer timesteps using round(max(0, delta_d)/Delta t_m).
2:	Tighten EV effective departure windows while preserving at least one timestep after arrival.
3:	Increase EV planning energy using the fixed heuristic reserve factor in Equation (9); apply path-specific feasibility fallback/capping.
4:	Stress building/TCL thermal planning with the fixed heuristic heat/dropout transformation in Equation (10).
5:	Use service-constrained building control when an agent is dropped, or the dropout sensitivity reaches the fallback threshold.
6:	Audit dispatch under the separate EV earlier-departure stress case; the implemented metric stress_comfort_violation_degree_minutes is recorded as zero.

3.5. Experimental Design

The study uses a 24 h horizon with 15 min timesteps. Synthetic EV and building agents are generated from deterministic seeds. Placement controls include penetration level, clustered versus dispersed adoption, phase policy, EV location class, and building type. The simplified radial feeder is used for controlled algorithmic comparisons when no OpenDSS model is part of the run.

OpenDSS feeder evaluation uses locally configured IEEE 123 and IEEE 34 feeder master files. The adapter compiles the feeder for each timestep, discovers native load buses and phases, scales feeder-native loads to the scenario base load, injects each individual EV/building AgentLoad at mapped service points, solves snapshot power flow, and records native voltage, line-loading, transformer-loading, phase-imbalance, losses, and service-location diagnostics. OpenDSS is therefore an ex-post feeder audit/evaluation layer. Its voltage and loading results are not embedded as hard constraints in every scheduler and are not a formal security certification.

The experimental design is summarized in Table 2. The simplified radial study isolates controller behavior under controlled uncertainty factors. The IEEE 123 and IEEE 34 OpenDSS uncertainty matrices provide the main feeder-physics evidence using the uncertainty settings configured at the time of the long feeder runs. Focused data-minimization, conformal-margin, and optimization-aware experiments are intentionally narrower because they test specific scientific claims rather than universal performance.

Table 2. Scenario factors and analytical role.

Study	Scenario Factors and Analytical Role
Controller behavior	Simplified radial benchmark; uncontrolled, service-constrained, feeder-aware, and uncertainty-aware modes; 256 scenarios from two seeds and 1024 controller evaluations; 50% EV/building penetration; dispersed/clustered adoption; balanced phase policy; workplace and mixed EV classes; EV arrival/departure, requested-energy error, outdoor-temperature shift, and dropout factors. Supports controller-behavior and service-grid tradeoff evidence; feeder physics is evaluated in the OpenDSS matrices.
OpenDSS matrices	IEEE 123 and IEEE 34 OpenDSS engines; same four controller modes; 2048 scenarios and 8192 controller evaluations per feeder from two seeds; 50% penetration; dispersed/clustered adoption; balanced/random phase policies; workplace/mixed EV classes; residential/mixed building classes; same factor structure with configured stress magnitudes at run time. Main evidence for feeder-specific voltage, loading, phase, and placement effects.
Information views	Simplified radial, IEEE 123, and IEEE 34; raw-state, individual-contract, and noisy/coarsened information-view proxies; one seeded short case per feeder/view; clustered adoption; balanced phase policy; fixed EV/building class mix; fixed information-view stress case. Supports exposure and serialized-payload proxy comparison; no formal privacy mechanism is implemented.
Conformal margins	Simplified radial, IEEE 123, and IEEE 34; four historical controller modes; three margin levels per feeder; clustered adoption; balanced phase policy; fixed EV/building class mix; 80/90/95% split-conformal scalar service-score margins. Supports marginal scalar-score coverage diagnostics and reserve-cost trends; feeder-wide probabilistic voltage and loading security are evaluated separately through OpenDSS diagnostics.
Optimization-aware	IEEE 123 and IEEE 34 OpenDSS engines; feeder-aware, uncertainty-aware, optimization-aware, and baseline modes; eight paired scenarios from two seeds and 40 evaluations; dispersed/balanced and clustered/random placement cases; selected EV departure, requested-energy, and heat-stress factors. Supports a bounded linearized controller scaffold for reserve and feeder-stress co-tuning; AC OPF benchmarking is a future comparison.

The identical service-risk counts reported for IEEE 123 and IEEE 34 follow from the experiment design. The stress-risk audit is driven by the shared synthetic service cases and uncertainty perturbations, so the same agent-service scenario can produce the same stress-risk count on both feeders. Feeder voltage, line-loading, transformer-loading, phase-imbalance, and service-location metrics are then computed using feeder-specific OpenDSS models; the resulting grid impacts differ because the two feeders have different impedances, native load locations, phase structure, and service-point mappings. The historical simplified-feeder stress-risk reduction reported in Results should be interpreted as an EV earlier-departure stress-audit result: the implemented metric stress_comfort_violation_degree_minutes is recorded as zero.

3.6. Empirical and Split-Conformal Input Selection

Empirical uncertainty inputs are constructed outside the controller and written into experiment configuration keys. EV arrival, early-departure, and requested-energy quantities use ACN charging-session fields as service residual proxies; outdoor-temperature uncertainty uses weather persistence residuals; thermal service uncertainty uses a reduced-order thermal-model error proxy from National Renewable Energy Laboratory (NREL)/National Institute of Standards and Technology (NIST)-style calibration artifacts. These inputs populate scenario or controller uncertainty keys, but they do not estimate the fixed structural coefficients in Equations (8)–(11). Communication dropout remains a configured sensitivity assumption rather than a telemetry-calibrated quantity.

The split-conformal extension is a scalar service-score input-selection procedure. The executable calibration uses a split seed of 20260727, confidence levels of 80%, 90%, and 95%, and train/calibration/test-type partitions formed by shuffling with deterministic seeds. For EV session records, the split fractions are 60% training, 20% calibration, and the remaining records for held-out testing. The score families are arrival-time deviation, early-departure service risk, requested-energy shortfall fraction, and thermal comfort heat stress. Thermal scores use weather heat residuals plus a reduced-order thermal root-meansquare error (RMSE) proxy and apply a separate deterministic seed offset for the value split. For a calibration score set of size n and confidence level $c = 1 - \alpha$, the finite-sample conformal quantile uses rank

$$r = \lceil (n + 1)c \rceil, \tag{15}$$

with the largest available calibration score used as a fallback when the rank exceeds n. The selected scalar quantiles are mapped into the existing uncertainty keys: EV arrival minutes, EV early-departure minutes, EV requested-energy shortfall fraction, and thermal-model error. The procedure provides finite-sample marginal coverage for those scalar scores under exchangeability assumptions; it is not a new conformal algorithm, not a joint EV/building guarantee, not conditional coverage, not a feeder-security guarantee, and not a learned controller reserve law.

3.7. Information-View and Noisy/Coarsened Protocol

The reduced-information experiment is an information-view and information-exposure proxy study. It uses the privacy-utility configurations with a 24 h horizon, 15 min timestep, seed 20260724, 60 EV agents, 60 building/TCL agents, clustered placement, balanced phase policy, and the three information levels raw_data_oracle, contract_only, and noisy_contract_aggregation. These labels describe serialized accounting views; in all three levels, dispatch is still built by calling the feeder-aware scheduler on a SmokeScenario and a feeder-sensitivity view.

The raw-state view serializes per-agent EV and building private-state records for accounting. The EV raw record includes agent identifier (ID), bus, phase, arrival step, departure step, battery capacity, initial SOC, target SOC, requested energy, charger rating, and location class. The building raw record includes agent ID, bus, phase, base load, HVAC rating, initial temperature, comfort bounds, thermal gain, cooling coefficient, and building type.

The individual-contract information view serializes the generated EV and building-contract dictionaries. This payload includes time-indexed min/max envelopes and service fields, which is why its byte count can exceed that of the raw-state payload, even though the exposure proxy assigns a lower semantic weight to contract fields. The label contract_only in saved artifacts should be read as an individual-contract payload/exposure proxy, not as proof that the executable controller receives only serialized contracts.

The noisy/coarsened information-view proxy has three separate mechanisms. First, dispatch planning uses a noised base-load profile $\hat{P}_t^0 = \max\{0, P_t^0(1 + \xi_t)\}$ with independent Gaussian $\xi_t \sim \mathcal{N}(0, 0.02^2)$ and seed offset seed + 1907. Second, the feeder-sensitivity view is coarsened to zone granularity and perturbed by per-bus Gaussian noise with standard deviation 0.08 and seed offset seed + 3401, then clipped to a minimum sensitivity of 0.1. Third, generated contracts are concatenated as EV contracts followed by building contracts and grouped into sequential chunks of nominal size 10, producing 12 groups for the 120-agent privacy-utility case. The grouped payload stores group_id, agent_count, location_granularity, and per-timestep min_kw and max_kw. Each grouped min/max value is independently perturbed by Gaussian noise with standard deviation 0.15 kW using seed offset seed + 8123, clipped at zero, and rounded to three decimals before JavaScript Object Notation (JSON) serialization.

Only the first two mechanisms affect dispatch planning. The grouped/noisy contract-envelope payload is used for exposure and payload accounting, either after or alongside dispatch, and is not consumed as a dispatch input. No feasibility projection is applied to the grouped/noisy envelopes beyond nonnegative clipping; independently noised min/max fields are therefore not claimed to be physically feasible dispatch bounds. The observed noisy-view utility degradation should be interpreted as arising from degraded base-load planning information and noised/coarsened feeder sensitivity, not from dispatching noised grouped contract envelopes.

3.8. Metrics and Scope of Inference

Grid metrics are computed from feeder-evaluation step results. They include peak load, losses, voltage violations below the configured minimum voltage limit, overload indicators above 100% loading, line-overload timesteps, transformer-overload timesteps, maximum line loading, maximum transformer loading, and maximum phase imbalance. Service metrics are ex-post nominal realized metrics: EV departure-energy shortfall, EV departure-SOC violation count, building comfort degree-minutes, and emergency-override count. Stress-audit service-risk flags are separate from nominal realized service metrics; they are based on stress EV shortfall or stress comfort violation fields in controller metrics.

The information-exposure score is a project-defined proxy,

$$X = F_{\text{private}} + 0.25F_{\text{contract}} + L_{\text{loc}}N_{\text{agent}}, \quad (16)$$

where F_{private} is the counted number of shared raw private fields, F_{contract} is the counted number of shared contract fields, L_{loc} is the location-granularity score, and N_{agent} is the number of EV plus building agents. Exact bus/phase location uses $L_{\text{loc}} = 1.0$; zone granularity uses $L_{\text{loc}} = 0.35$; system granularity uses $L_{\text{loc}} = 0.0$; otherwise, the implementation uses 0.5. This is not measured information leakage, mutual information, a differential-privacy epsilon, or a formal privacy metric.

Serialized payload size is also an accounting proxy. The implementation forms deterministic JavaScript Object Notation (JSON) strings with sorted keys for the raw, individual-contract, or grouped/noisy payload and records len(payload.encode("utf-8")). This is a serialized payload-size proxy; it does not measure network traffic, bandwidth, or end-to-end communication overhead. Conformal coverage metrics are held-out scalar-score coverage diagnostics and do not imply feeder-wide voltage, loading, or service feasibility guarantees.

4. Results

4.1. Results Overview and Scope

Table 3 summarizes the main results, their supporting experiments, and the scope of inference.

Table 3. Summary of results and scope of inference.

Result	Supporting Experiment and Quantitative Outcome	Scope of Inference
Across tested nominal synthetic scenarios, realized EV departure-energy shortfall and building comfort violations are zero.	Controller-behavior matrix reports 0 realized EV energy shortfall and 0 comfort violations; the OpenDSS runs use the same nominal service audit.	Tested synthetic scenarios and service-audit definitions.
Earlier-departure EV stress-audit protection has a peak cost.	Implemented stress-audit flags fall 106 to 64 in the simplified matrix and 1005 to 536 on both OpenDSS feeders; mean peak cost is 33.78 kW in the simplified matrix and 17.66/18.26 kW on IEEE 123/34.	Earlier-departure EV stress audit under configured uncertainty factors.
OpenDSS feeder outcomes differ by feeder.	OpenDSS overload-delta totals are 1152 on IEEE 123 and 3746 on IEEE 34; voltage-delta totals are 0 and 2.	Two locally configured IEEE feeders; ex-post OpenDSS diagnostics.
Individual-contract information views reduce the exposure proxy in a focused comparison.	The individual-contract information view matches the raw-state information view's peak reduction on both feeders, while the information-exposure proxy score falls from 1260 to 495; the noisy/coarsened information view lowers the score to 63 but costs about 69–70 kW.	Focused short utility checks using information-exposure and serialized payload-size proxies; grouped/noisy payloads are not dispatch inputs.
Split-conformal scalar service-score inputs reveal reserve-cost sensitivity.	At 95%, stress shortfall reduction is 412.18 kWh; peak cost is 118.63 kW on IEEE 123 and 124.40 kW on IEEE 34.	Scalar service-score input sensitivity with ex-post OpenDSS diagnostics.

Optimization-aware allocation clarifies the tested tradeoff.	Optimization-aware mode removes stress-risk flags in the tested cases but increases peak tradeoff; IEEE 34 overload exposure rises under selected weights.	Focused linearized allocation analysis with OpenDSS feeder audit.

4.2. Realized Service Outcomes

Across the tested nominal synthetic scenarios, realized EV departure-energy shortfall and building comfort violations were zero. In the 256-scenario controller-behavior matrix, the maximum realized EV energy shortfall is 0 kWh, and the maximum comfort violation is 0 degree-minutes. The separate stress audit asks whether the same EV schedules still satisfy earlier-departure service tests under uncertainty perturbations. That audit is where the service-grid tradeoff appears. Table 4 summarizes the controller-mode service and peak outcomes.

Table 4. Controller-mode service and peak-outcome variation.

Mode	Cases	Seeds	Peak Mean	Peak Std	Peak-Red. Mean	Peak-Red. Range	Stress-Risk
Uncontrolled	256	2	1562.7	50.10	0.00	0.00 to 0.00	0
Service-constrained	256	2	1519.9	32.06	42.79	−14.20 to 144.39	0
Feeder-aware	256	2	1477.4	35.54	85.33	17.02 to 192.34	106
Uncertainty-aware	256	2	1511.2	50.23	51.55	−27.69 to 166.07	64

4.3. Service-Risk Reduction and Peak-Cost Tradeoff

The simplified matrix quantifies a measurable earlier-departure EV stress-risk/peak-reduction tradeoff: stress-audit flags fall from 106 to 64 while mean peak reduction falls from 85.33 to 51.55 kW, corresponding to a 33.78 kW mean peak cost. Deterministic feeder-aware dispatch reduces peak more aggressively, while the heuristic uncertainty-aware mode reserves EV energy and building thermal flexibility according to the implemented uncertainty rules. Table 4 also shows substantial scenario variation: uncertainty-aware peak reduction ranges from −27.69 kW to 166.07 kW, so the reserve policy can be costly in some cases and useful in others. Figures 2 and 3 report the two-feeder OpenDSS uncertainty-study outcomes discussed in Section 4.4; they do not depict the separate 256-scenario simplified matrix summarized above.

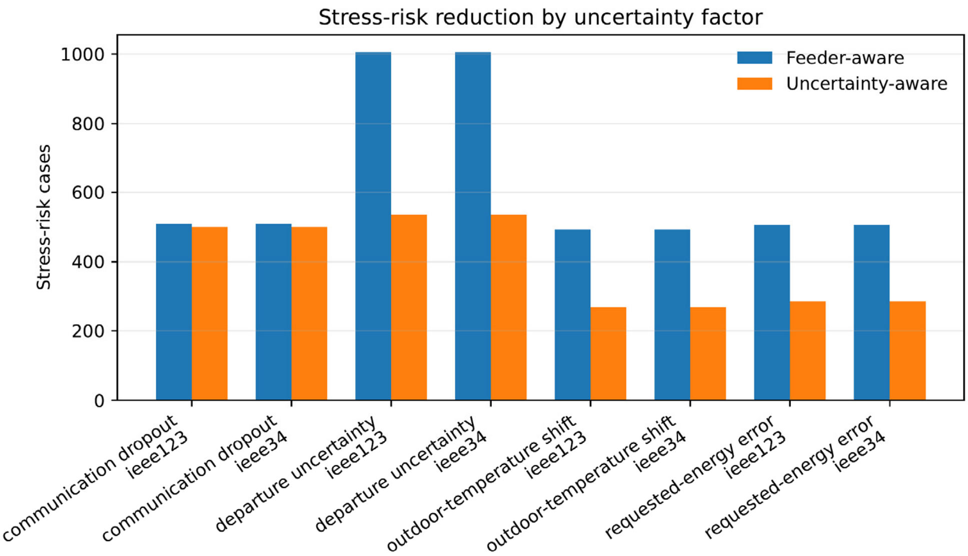

Figure 2. Earlier-departure EV stress-audit case counts by nonzero uncertainty factor for feeder-aware and uncertainty-aware control in the IEEE 123 and IEEE 34 OpenDSS studies; each bar summarizes 1024 paired scenarios.

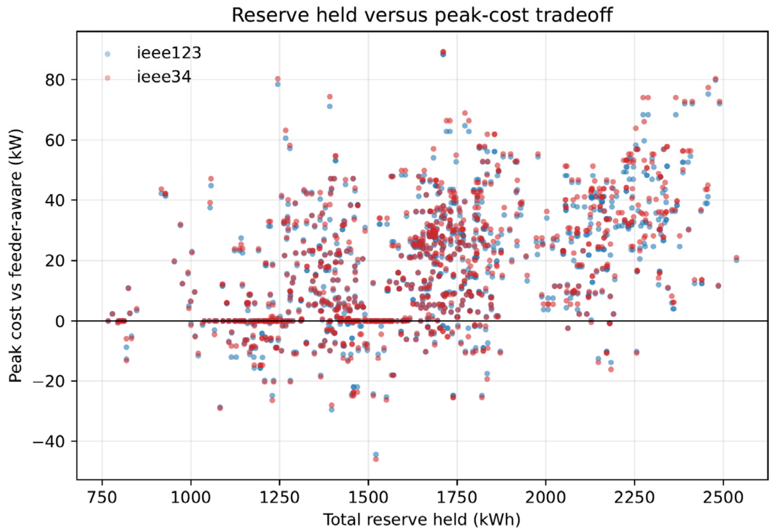

Figure 3. Total EV-plus-thermal reserve held under uncertainty-aware control versus peak-demand cost relative to feeder-aware control in the IEEE 123 and IEEE 34 OpenDSS studies; each feeder contributes 2048 paired scenarios.

4.4. Feeder-Physics Impacts on IEEE 123 and IEEE 34

The OpenDSS uncertainty studies provide the primary ex-post feeder audit evidence. Each IEEE feeder has 2048 scenarios and 8192 controller evaluations using the uncertainty settings available at the time of the long feeder runs. The two-feeder OpenDSS comparison shows feeder-dependent peak, overload, and voltage outcomes for the same stress-audit count reduction, from 1005 to 536 cases on both IEEE 123 and IEEE 34. The mean peak tradeoff relative to deterministic feeder-aware dispatch is similar across feeders, but the feeder-loading outcome is not: the overload-delta total is 1152 on IEEE 123 and 3746 on IEEE 34. This difference is central to the paper. The same heuristic uncertainty-aware policy can have different ex-post feeder outcomes when feeder impedance, loading, phase structure, and service-point mapping change. Table 5 summarizes the two-feeder service-grid tradeoff.

Table 5. IEEE 123 and IEEE 34 service-grid tradeoff.

Feeder	Cases	Cost Mean	Cost Min	Cost Max	Cost Std	Resolved	Overload Delta	Voltage Delta
IEEE 123	2048	17.66	−44.34	88.32	19.62	469	1152	0
IEEE 34	2048	18.26	−45.93	89.14	20.33	469	3746	2

Figure 4 shows the corresponding loading-duration curves for the two OpenDSS feeders.

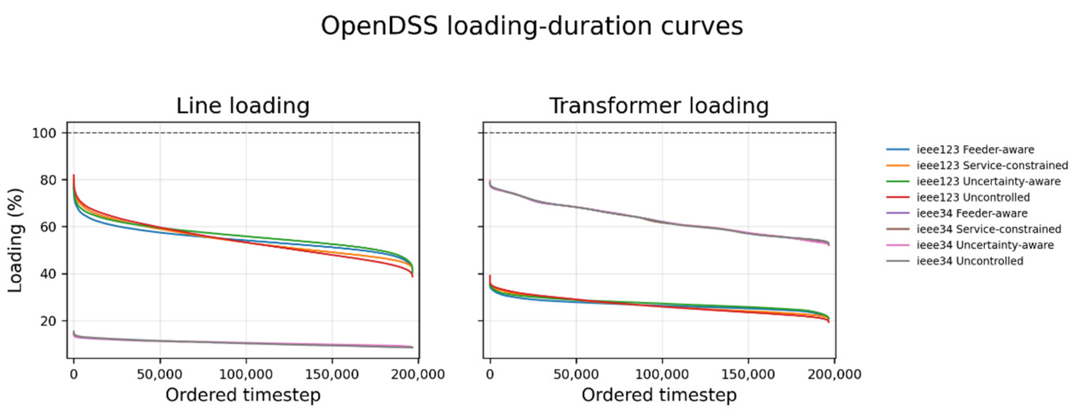

Figure 4. OpenDSS (Open Distribution System Simulator) loading-duration curves for IEEE 123 and IEEE 34 ex-post feeder audits.

Clustered and dispersed adoption produce similar stress-audit reductions but different feeder-stress patterns. In the OpenDSS uncertainty matrices, clustered adoption has a higher mean peak cost and larger overload-delta totals than dispersed adoption on both feeders. Native feeder-physics diagnostics also show that IEEE 34 has lower voltage headroom and higher transformer-loading exposure than IEEE 123 under the mapped service points. These observations motivate future objective tuning that accounts for service reserve, feeder-specific loading, and phase concentration.

4.5. Information-View Proxy Tradeoff

The reduced-information contribution is evaluated through an information-view proxy comparison. Table 6 compares raw-state, individual-contract, and noisy/coarsened information views on IEEE 123 and IEEE 34. In the focused information-view comparison, the individual-contract view exactly matched raw-state peak reduction on both feeders while lowering the information-exposure proxy from 1260 to 495. The serialized payload-size proxy is larger for the individual-contract view because it contains time-indexed envelopes. The noisy/coarsened information view reduces serialized payload size and the exposure proxy further, but produces a 69.24 kW peak tradeoff on IEEE 123 and a 70.15 kW peak tradeoff on IEEE 34, with a 6.50 kWh stress-audit EV shortfall. That utility change should be read as the effect of degraded/noised base-load planning information and noised/coarsened feeder sensitivity; the grouped/noisy contract-envelope payload is serialized for accounting and is not consumed as a dispatch input.

Table 6. OpenDSS (Open Distribution System Simulator) information-view proxy comparison.

Feeder	Information View	Peak Red. (kW)	Tradeoff (kW)	Stress Shortfall (kWh)	Serialized Payload (kB)	Exposure Proxy
IEEE 123	Raw-state view	60.15	0.00	0.00	38.15	1260
IEEE 123	Individual-contract view	60.15	0.00	0.00	375.13	495
IEEE 123	Noisy/coarsened view	−9.08	69.24	6.50	17.27	63
IEEE 34	Raw-state view	60.82	0.00	0.00	38.15	1260
IEEE 34	Individual-contract view	60.82	0.00	0.00	375.13	495
IEEE 34	Noisy/coarsened view	−9.33	70.15	6.50	17.27	63

Figure 5 summarizes the exposure and payload proxy comparison for the focused reduced-information test.

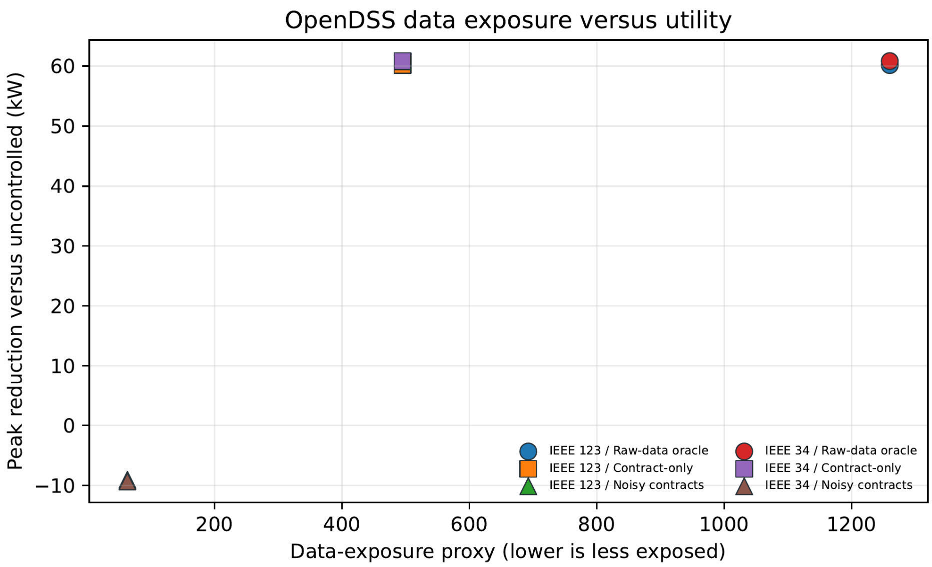

Figure 5. Information-view exposure and serialized payload-size proxy comparison for raw-state, individual-contract, and noisy/coarsened views in the focused reduced-information comparison.

4.6. Calibrated and Conformal Service-Margin Cost

Empirical EV margins use a partial ACN-Data multi-site merge, weather persistence residuals, and National Renewable Energy Laboratory (NREL)/National Institute of Standards and Technology (NIST) thermal calibration outputs. The conformal-input study shows that higher split-conformal scalar service-score quantile levels increase reserve cost and stress-shortfall reduction in the tested OpenDSS audits. Table 7 reports the corresponding OpenDSS feeder impacts. At 95%, stress shortfall reduction reaches 412.18 kWh on both feeders, while peak cost reaches 118.63 kW on IEEE 123 and 124.40 kW on IEEE 34. These are conformal-input sensitivity results for scalar service-score quantile inputs.

Table 7. OpenDSS (Open Distribution System Simulator) split-conformal scalar service-score input impacts.

Feeder	Level	Peak Cost (kW)	Shortfall Reduction (kWh)	EV Reserve (kWh)	Overload Delta
IEEE 123	80%	79.43	122.44	278.30	4
IEEE 123	90%	105.27	223.15	278.30	6
IEEE 123	95%	118.63	412.18	278.30	6
IEEE 34	80%	79.93	122.44	278.30	4
IEEE 34	90%	109.22	223.15	278.30	9
IEEE 34	95%	124.40	412.18	278.30	13

Figure 6 shows the peak-cost pattern for the split-conformal scalar service-score inputs.

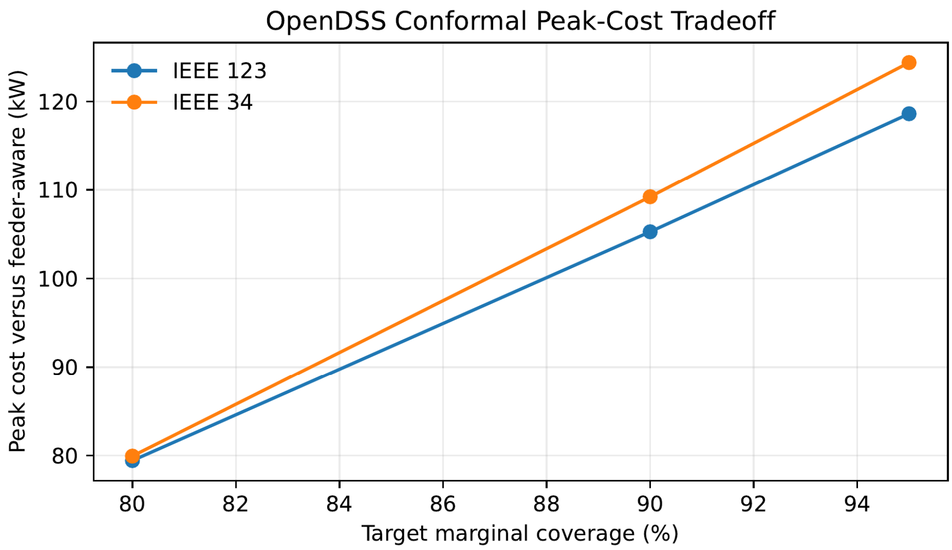

Figure 6. Peak-cost comparison for split-conformal scalar service-score inputs in the OpenDSS feeder audits on IEEE 123 and IEEE 34.

4.7. Optimization-Aware Allocation Results

The optimization-aware controller is included to make the coordination objective explicit in a focused analysis. It retains individual EV/time decision variables and individual building profiles, while the bus/phase contract count enters the EV cost as a location-density term. The allocation problem is linearized and is solved with SciPy linear programming or a deterministic fallback; nonlinear feeder feasibility is evaluated ex post through OpenDSS rather than guaranteed by the scheduler. Table 8 shows the bounded IEEE 123/IEEE 34 optimization-aware study. The focused linearized allocation study shows that reducing tested stress-risk flags to zero can increase peak tradeoff and, on IEEE 34 under the selected weights, overload-count exposure. This result identifies reserve cost, phase concentration, and feeder loading as coupled design variables for future objective tuning.

Table 8. Linearized optimization-aware two-feeder OpenDSS (Open Distribution System Simulator) audit.

Feeder	Mode	Cases	Peak Red. (kW)	Tradeoff (kW)	Risk Cases	Overload Viol.
IEEE 123	Feeder-aware	4	44.29	0.00	1	0
IEEE 123	Uncertainty-aware	4	32.65	11.64	0	0
IEEE 123	Optimization-aware	4	32.37	11.92	0	0
IEEE 34	Feeder-aware	4	44.58	0.00	1	0
IEEE 34	Uncertainty-aware	4	32.96	11.62	0	1
IEEE 34	Optimization-aware	4	27.69	16.89	0	8

Figure 7 shows the focused optimization-aware controller tradeoff across the two feeders.

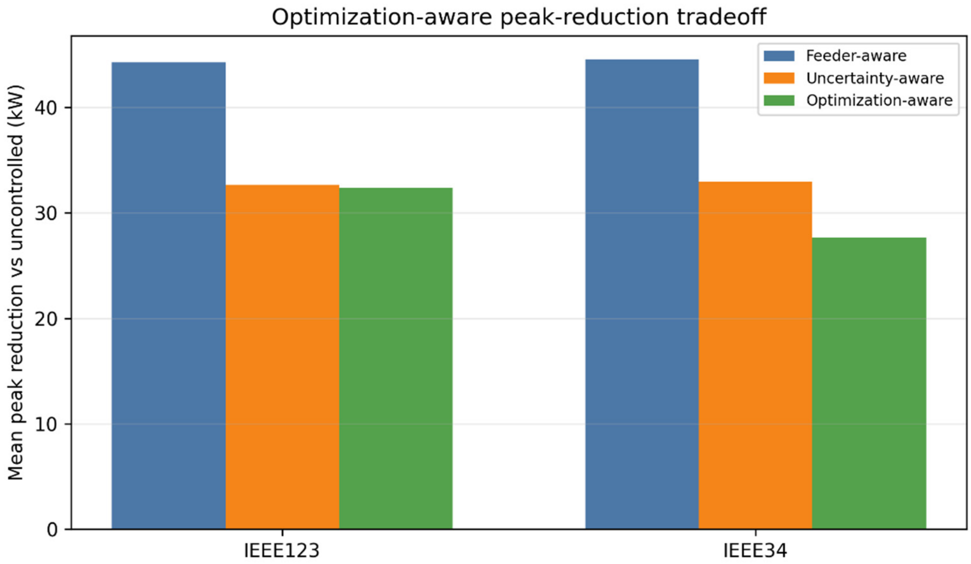

Figure 7. Linearized optimization-aware controller tradeoff on IEEE 123 and IEEE 34 under the focused two-feeder OpenDSS audit.

5. Discussion

The results support a bounded empirical interpretation: the shared EV/building service-contract representation exposes tradeoffs among realized service outcomes, earlier-departure EV stress-audit outcomes, feeder loading and voltage outcomes, reduced-information information views, and heuristic uncertainty inputs. Across the tested nominal synthetic scenarios, realized EV departure-energy shortfall and building comfort violations were zero. In the separate simplified stress audit, heuristic uncertainty-aware tightening reduces earlier-departure EV stress-audit flags from 106 to 64, with a 33.78 kW mean peak cost relative to deterministic feeder-aware dispatch. These outcomes show a service-grid tradeoff in the evaluated cases.

The two OpenDSS feeder audits strengthen this interpretation. IEEE 123 and IEEE 34 show the same implemented stress-audit reduction, from 1005 to 536 cases, but different overload behavior: overload-delta totals are 1152 on IEEE 123 and 3746 on IEEE 34. Controller performance under mapped individual-agent loads, therefore, depends on feeder topology, phase structure, native loading, and service-point placement. The reduced-information experiment adds an empirical information-view tradeoff. The individual-contract information view matches the raw-state information view's peak reduction on both feeders while reducing the information-exposure proxy from 1260 to 495. The noisy/coarsened information view further reduces the exposure proxy and the serialized payload-size proxy, but its utility degradation should be attributed to noisy/degraded base-load planning information and noisy/coarsened feeder sensitivity; the grouped/noisy contract-envelope payload is not a dispatch input.

The empirical and conformal margin experiments sharpen the interpretation of uncertainty without changing its scope. Empirical confidence labels are operational controller settings derived from available residual data. Split-conformal margins provide finite-sample marginal score coverage for specified scalar service scores under exchangeability, while feeder-wide voltage and loading outcomes remain ex-post OpenDSS feeder-audit results. The optimization-aware analysis likewise has a focused role: it provides a linearized optimization-aware EV allocation scaffold with individual EV/time variables, individual building profiles, SciPy linear programming or deterministic fallback, and a bus/phase contract-count location-density cost term. It is useful for testing reserve and feeder-stress objective weights, not for claiming AC OPF or guaranteed nonlinear feeder feasibility.

6. Scope, Limitations, and Future Work

These contributions are scoped around a clear technical boundary. The current implementation is a monolithic individual-agent simulator: service contracts, bus/phase summaries, information-view records, exposure quantities, and payload quantities are representation and evaluation objects, not the exclusive controller boundary. No true contract-only, aggregate-only, or noisy grouped-contract dispatch architecture is implemented. The study evaluates reduced-information representations that could reduce exposed information relative to raw-state views, while the executable simulator retains individual agent state internally.

The information-view results are proxy measurements. The information-exposure score is a declared-field and location-granularity proxy, not measured leakage, mutual information, a differential-privacy budget, or a formal privacy metric. The payload values are serialized payload-size accounting from deterministic JSON, not measured bandwidth, latency, or communication cost. The grouped/noisy contract-envelope payload is serialized for exposure and payload accounting and is not consumed by dispatch. In the noisy/coarsened view, dispatch changes come from noised/degraded base-load planning information and noised/coarsened feeder sensitivity.

The feeder and uncertainty evidence is also bounded. IEEE 123 and IEEE 34 provide complementary OpenDSS ex-post feeder evaluation with synthetic agents and 24 h scenarios; they do not establish universal feeder generality or a feeder-security certificate. The uncertainty-aware controller uses fixed heuristic coefficients and configured or empirically populated uncertainty inputs; these coefficients are design heuristics, not learned laws. The split-conformal component supplies scalar service-score uncertainty inputs under exchangeability assumptions only. It does not provide joint EV/building, conditional, or feeder-wide voltage/loading guarantees. The historical 106 to 64 result should be read as an earlier-departure EV stress-audit flag reduction; the implemented metric stress_comfort_violation_degree_minutes is recorded as zero.

The optimization-aware analysis is a linearized scaffold rather than AC OPF. Individual EV/time variables and individual building profiles remain in the analysis, the bus/phase contract count enters as a location-density cost term, SciPy linear programming or a deterministic fallback solves the EV allocation, and OpenDSS is used afterward for feeder evaluation.

Future work should implement and test stronger methods directly. Useful extensions include a true contract-only executable controller; aggregate-only or hierarchical contract dispatch; formal differential privacy, secure aggregation, or other threat-model-driven privacy mechanisms; feasible noisy-envelope projection; true grouped-contract dispatch experiments; nonlinear AC OPF or robust network constraints; joint EV/building stress testing; field or live-data integration; operational digital-twin synchronization; and telemetry-calibrated communication-dropout models. These are future extensions rather than capabilities demonstrated by the present implementation.

7. Conclusions

This paper presents and empirically evaluates two main contributions. First, it implements a shared service-enriched EV/building representation that encodes EV departure-energy/deadline service and building comfort/thermal service with feeder bus/phase labels and summaries inside an individual-agent feeder workflow. Second, it empirically evaluates how the shared representation exposes service-grid, uncertainty-input, feeder-audit, and information-view tradeoffs across the simplified and OpenDSS feeder studies.

The main empirical pattern is a bounded service-grid tradeoff. Across the tested nominal synthetic scenarios, realized EV departure-energy shortfall and building comfort violations were zero. The separate simplified stress audit shows an earlier-departure EV stress-audit flag reduction from 106 to 64 at a 33.78 kW mean peak cost. In the OpenDSS feeder audits, implemented stress-audit cases fell from 1005 to 536 on both IEEE 123 and IEEE 34, with mean peak costs of 17.66 kW and 18.26 kW and feeder-specific overload outcomes.

The information-view results foreground the value of comparing representation choices directly. The individual-contract information view matches raw-state peak reduction on both feeders while reducing the exposure proxy from 1260 to 495; the noisy/coarsened view further reduces exposure and payload, with utility changes driven by noisy base-load planning information and noisy/coarsened feeder sensitivity rather than dispatch from grouped/noisy contract envelopes. The split-conformal inputs and optimization-aware analysis provide scalar service-score sensitivity and a focused linearized allocation study within the same empirical evaluation. Overall, the findings provide bounded empirical evidence for using shared EV/building service representations to study contract-only control, formal privacy mechanisms, and feeder-constrained optimization as future extensions.

Statement of the Use of Generative AI and AI-Assisted Technologies in the Writing Process

During the preparation of this manuscript, the authors used OpenAI ChatGPT to assist with language editing. After using this tool, the authors reviewed and edited the content as needed and take full responsibility for the content of the submitted manuscript.

Author Contributions

Conceptualization, D.O. and E.G.; Methodology, D.O., E.G. and F.M.I.; Software, D.O.; Validation, D.O. and F.M.I.; Formal Analysis, D.O.; Investigation, D.O.; Data Curation, D.O.; Writing—Original Draft Preparation, D.O.; Writing—Review and Editing, D.O., E.G. and F.M.I.; Visualization, D.O.; Supervision, E.G. and F.M.I.; Project Administration, E.G.; Funding Acquisition, not applicable. All authors have read and agreed to the submitted version of the manuscript.

Ethics Statement

Not applicable. This study uses synthetic EV and building/TCL agents and public feeder models and does not involve human participants, animals, or identifiable private records.

Informed Consent Statement

Not applicable.

Data Availability Statement

The author-generated simulation outputs, experiment configurations, and processed calibration artifacts supporting the results of this study are available from the corresponding author upon reasonable request. Third-party datasets and feeder models used in this study should be obtained from their original providers.

Funding

This research received no external funding. No external article-processing-charge (APC) funding was received.

Declaration of Competing Interest

The authors declare that they have no known competing financial interests or personal relationships that could have appeared to influence the work reported in this paper.

Code Availability

The author-developed source code used for the simulations and analyses reported in this study is available from the corresponding author upon reasonable request.

References

1. Clement-Nyns K, Haesen E, Driesen J. The impact of charging plug-in hybrid electric vehicles on a residential distribution grid. *IEEE Trans. Power Syst.* **2010**, *25*, 371–380. DOI:10.1109/TPWRS.2009.2036481
2. Pieltain Fernandez L, Gomez San Roman T, Cossent R, Mateo Domingo C, Frias P. Assessment of the impact of plug-in electric vehicles on distribution networks. *IEEE Trans. Power Syst.* **2011**, *26*, 206–213. DOI:10.1109/TPWRS.2010.2049133
3. Dubey A, Santoso S. Electric vehicle charging on residential distribution systems: impacts and mitigations. *IEEE Access* **2015**, *3*, 1871–1893. DOI:10.1109/ACCESS.2015.2476996
4. Muratori M. Impact of uncoordinated plug-in electric vehicle charging on residential power demand. *Nat. Energy* **2018**, *3*, 193–201. DOI:10.1038/s41560-017-0074-z
5. Mu Y, Wu J, Jenkins N, Jia H, Wang C. A spatial-temporal model for grid impact analysis of plug-in electric vehicles. *Appl. Energy* **2014**, *114*, 456–465. DOI:10.1016/j.apenergy.2013.10.006
6. Quiros-Tortos J, Ochoa LF, Alnaser SW, Butler T. Control of EV charging points for thermal and voltage management of LV networks. *IEEE Trans. Power Syst.* **2016**, *31*, 3028–3039. DOI:10.1109/TPWRS.2015.2468062
7. Gan L, Topcu U, Low SH. Optimal decentralized protocol for electric vehicle charging. *IEEE Trans. Power Syst.* **2013**, *28*, 940–951. DOI:10.1109/TPWRS.2012.2210288
8. Hu J, You S, Lind M, Ostergaard J. Coordinated charging of electric vehicles for congestion prevention in the distribution grid. *IEEE Trans. Smart Grid* **2014**, *5*, 703–711. DOI:10.1109/TSG.2013.2279007
9. Lee ZJ, Li T, Low SH. ACN-Data: Analysis and applications of an open EV charging dataset. In *Proceedings of the Tenth ACM International Conference on Future Energy Systems, Phoenix, AZ, USA, 25–28 June 2019*; ACM: New York, NY, USA, 2019; pp. 139–149. DOI:10.1145/3307772.3328313
10. Lee ZJ, Sharma S, Johansson D, Low SH. ACN-Sim: An open-source simulator for data-driven electric vehicle charging research. *IEEE Trans. Smart Grid* **2021**, *12*, 5113–5123. DOI:10.1109/TSG.2021.3103156
11. Sadeghianpourhamami N, Refa N, Strobbe M, Develder C. Quantitive analysis of electric vehicle flexibility: A data-driven approach. *Int. J. Electr. Power Energy Syst.* **2018**, *95*, 451–462. DOI:10.1016/j.ijepes.2017.09.007
12. Huber J, Dann D, Weinhardt C. Probabilistic forecasts of time and energy flexibility in battery electric vehicle charging. *Appl. Energy* **2020**, *262*, 114525. DOI:10.1016/j.apenergy.2020.114525
13. Yan D, Ma C, Chen Y. Distributed coordination of charging stations considering aggregate EV power flexibility. *IEEE Trans. Sustain. Energy* **2023**, *14*, 356–370. DOI:10.1109/TSTE.2022.3213173
14. Winschermann L, Banol Arias N, Hoogsteen G, Hurink JL. Assessing the value of information for electric vehicle charging strategies at office buildings. *Renew. Sustain. Energy Rev.* **2023**, *185*, 113600. DOI:10.1016/j.rser.2023.113600
15. Callaway DS. Tapping the energy storage potential in electric loads to deliver load following and regulation, with application to wind energy. *Energy Convers. Manag.* **2009**, *50*, 1389–1400. DOI:10.1016/j.enconman.2008.12.012
16. Oldewurtel F, Parisio A, Jones CN, Gyalistras D, Gwerder M, Stauch V, et al. Use of model predictive control and weather forecasts for energy efficient building climate control. *Energy Build.* **2012**, *45*, 15–27. DOI:10.1016/j.enbuild.2011.09.022
17. Hao H, Sanandaji BM, Poolla K, Vincent TL. Aggregate flexibility of thermostatically controlled loads. *IEEE Trans. Power Syst.* **2015**, *30*, 189–198. DOI:10.1109/TPWRS.2014.2328865
18. Mathieu JL, Kamgarpour M, Lygeros J, Andersson G, Callaway DS. Arbitraging intraday wholesale energy market prices with aggregations of thermostatic loads. *IEEE Trans. Power Syst.* **2015**, *30*, 763–772. DOI:10.1109/TPWRS.2014.2335158

19. Coffman A, Busic A, Barooah P. A unified framework for coordination of thermostatically controlled loads. *Automatica* **2023**, *152*, 111002. DOI:10.1016/j.automatica.2023.111002
20. McKenna E, Richardson I, Thomson M. Smart meter data: Balancing consumer privacy concerns with legitimate applications. *Energy Policy* **2012**, *41*, 807–814. DOI:10.1016/j.enpol.2011.11.049
21. Erkin Z, Troncoso-Pastoriza JR, Lagendijk RL, Perez-Gonzalez F. Privacy-preserving data aggregation in smart metering systems: an overview. *IEEE Signal Process. Mag.* **2013**, *30*, 75–86. DOI:10.1109/MSP.2012.2228343
22. Hale M, Barooah P, Parker K, Yazdani K. Differentially Private Smart Metering: Implementation, Analytics, and Billing. In *Proceedings of the 1st ACM International Workshop on Urban Building Energy Sensing, Controls, Big Data Analysis, and Visualization*, *New York, NY, USA, 13 November 2019*; ACM: New York, NY, USA, 2019; pp. 33–42. DOI:10.1145/3363459.3363530
23. Palacios-Garcia EJ, Carpent X, Bos C, Deconinck G. Efficient privacy-preserving aggregation for demand side management of residential loads. *Appl. Energy* **2022**, *328*, 120112. DOI:10.1016/j.apenergy.2022.120112
24. Nosair H, Bouffard F. Flexibility envelopes for power system operational planning. *IEEE Trans. Sustain. Energy* **2015**, *6*, 800–809. DOI:10.1109/TSTE.2015.2410760
25. Liu B, Braslavsky JH. Robust dynamic operating envelopes for DER integration in unbalanced distribution networks. *IEEE Trans. Power Syst.* **2024**, *39*, 3921–3936. DOI:10.1109/TPWRS.2023.3308104
26. Liu G, Tao Y, Xu L, Chen Z, Qiu J, Lai S. Coordinated management of aggregated electric vehicles and thermostatically controlled loads in hierarchical energy systems. *Int. J. Electr. Power Energy Syst.* **2021**, *131*, 107090. DOI:10.1016/j.ijepes.2021.107090
27. Renkema Y, Brinkel N, AlSkaif T. Conformal prediction for stochastic decision-making of PV power in electricity markets. *Electr. Power Syst. Res.* **2024**, *234*, 110750. DOI:10.1016/j.epsr.2024.110750
28. Fan J, Kockar I. Three-phase OPF Based Local Flexibility Market for Mitigating Unbalanced Voltage in Distribution Systems. In Proceedings of the IEEE PES Innovative Smart Grid Technologies Europe (ISGT Europe), Espoo, Finland, 18–21 October 2021. DOI:10.1109/ISGTEurope52324.2021.9640000
29. Tostado-Veliz M, Hasanien HM, Siano P, Jurado F. Preference-aware flexibility envelopes for coordinated operation of energy communities. *Sustain. Energy Grids Netw.* **2026**, *47*, 102493. DOI:10.1016/j.segan.2026.102493
30. Roald LA, Pozo D, Papavasiliou A, Molzahn DK, Kazempour J, Conejo AJ. Power systems optimization under uncertainty: A review of methods and applications. *Electr. Power Syst. Res.* **2023**, *214*, 108725. DOI:10.1016/j.epsr.2022.108725
31. Cabrera-Tobar A, Blasuttigh N, Massi Pavan A, Spagnuolo G. Demand response of an Electric Vehicle charging station using a robust-explicit model predictive control considering uncertainties to minimize carbon intensity. *Sustain. Energy Grids Netw.* **2024**, *38*, 101381. DOI:10.1016/j.segan.2024.101381
32. Vovk V, Gammerman A, Shafer G. *Algorithmic Learning in a Random World*; Springer: New York, NY, USA, 2005. DOI:10.1007/b106715
33. Angelopoulos AN, Bates S. Conformal prediction: A gentle introduction. *Found. Trends Mach. Learn.* **2023**, *16*, 494–591. DOI:10.1561/2200000101
34. Electric Power Research Institute. OpenDSS Documentation: Examples, Documentation, and Test Cases. Available online: https://opendss.epri.com/ExamplesDocsandTestCases.html (accessed on 18 June 2026).
35. Kersting WH. Radial distribution test feeders. In *Proceedings of the IEEE Power Engineering Society Winter Meeting, Columbus, OH, USA, 28 January–1 February 2001*; IEEE: Piscataway, NJ, USA, 2001; pp. 908–912. DOI:10.1109/PESW.2001.916993
36. Arritt RF, Dugan RC. The IEEE 8500-node test feeder. In *Proceedings of the IEEE PES Transmission and Distribution Conference and Exposition*, *New Orleans, LA, USA, 19–22 April 2010*; IEEE: Piscataway, NJ, USA, 2010; pp. 1–6. DOI:10.1109/TDC.2010.5484381